Tabriz Journal of Electrical Engineering (TJEE), vol. 55, no. 1, 2025 Serial no. 111
DOI: 10.22034/tjee.2024.59687.4782

Analytical modelling of AlGaN/GaN HEMTs with p-layer in the barrier

R. Madadi[1]; S. E. Hosseini[2*]

[1,2] Electrical Engineering Department, Engineering Faculty, Ferdowsi University of Mashhad, Mashhad, Iran.
[1] ro.madadi@mail.um.ac.ir
[2] ehosseini@um.ac.ir
[*]Corresponding author

Received: 23/12/2023, Revised:30/05/2024, Accepted:03/07/2024.

Abstract
In this paper, we present a two-dimensional (2D) analytical modelling of a high electron mobility transistor (HEMT) with a p-layer in the barrier layer. In this model, the channel potential and electric field distributions are derived based on 2D Laplace equation, with Equivalent Potential Method (EPM) and appropriate boundary conditions, and under two assumptions of complete depletion/incomplete depletion. The EPM indicates that charges in the depletion region can be equated to a potential at passivation surface layer. This analytical model shows great simplicity and accuracy. It gives physical insights into the breakdown characteristics of the AlGaN/GaN HEMT with a p-layer in the barrier. This structure reduces the peak electric field at the gate corner near the drain and a new electric field peak is introduced by electric field modulation, which makes the electric field distribution of channel more uniform and, consequently increases the breakdown voltage of the device. The dependence of the channel potential and electric field distributions on length and thickness of the p-layer are investigated. The validity of this model is demonstrated by comparison with the numerical simulations using Silvaco-Atlas device simulator.

Keywords
Analytical model, Laplace Equations, Equivalent Potential Method (EPM), Potential, electric field, P-layer

1. Introduction

High electron mobility transistors (HEMTs) with high breakdown voltage, high carrier mobility, reduced impurity scattering, and superior thermal conductivity has become a dominant choice among transistors to be used in high temperature, high-frequency and high-power applications [1]. Wide-bandgap semiconductor materials exhibit many attractive properties far beyond the capabilities of silicon, such as high critical breakdown electric field strength, carrier drift velocity, high thermal conductivity, and large carrier mobility. These features result in increased breakdown voltage, large current density, and enhanced power density [2]. Gallium nitride (GaN) is one of the wide-bandgap semiconductor materials with good properties such as wide bandgap (≥3.4 eV), high breakdown field (3.5 MV/cm), high electron saturation speed (>2×10^7 cm/s) and high thermal conductivity which is suitable for power devices, especially AlGaN/GaN HEMTs [3], GaN power amplifiers [44] and GaN light-emitting diode [45]. High channel electron concentration (>1×10^{13} cm^{-2}) and high mobility (1000-2000 cm^2/V. s) 2D-electron gas (2DEG) at the AlGaN/GaN hetero-interface are generated by the spontaneous and piezoelectric polarization effects [4-10]. It can be found that in reverse bias, as the drain voltage increases, a high electric field peak appears at the gate edge of the drain side of an AlGaN/GaN HEMT, and the device breaks down when the electric field peak reaches the critical breakdown electric field of GaN material. Reducing the peak of the electric field at the edge of the gate, improving the breakdown voltage (BV) of the device and enhancing the nonuniform electric field distribution of AlGaN/GaN HEMTs are crucial. Based on the electric field modulation effect some techniques and methods are applied to get a high BV and high power density such as field plate [11-22], proton implantation [23], reduced-surface-field AlGaN/GaN with a double low-density drain and a positively charged region near the drain [24], partial silicon doping [25], partial GaN cap layer [26, 27] and so on [28-33]. All structures in [11-33] have been fabricated or numerically simulated, which cannot directly manifest the intrinsic mechanism to get a high BV characteristic of the device. By the way, the fabrications and experiments of AlGaN/GaN HEMTs are costly and time consuming [34]. It is known that the analytical method is an effective way to gain a physical insight into the breakdown characteristic of the device [35]. Some researchers have been proposed analytical models based on Poisson/Laplace equations for the potential and electric field distributions of AlGaN/GaN HEMT with field-plate [34, 36-39], partial silicon doping [40], GaN cap layer [41], and reduced-surface-field (RESURF) AlGaN/GaN HEMT [35], etched AlGaN layer [3].

Solving Poisson equation is difficult because of various charges in the device interfaces and the need for iterative calculation of a set of partial differential equations. Equivalent Potential Method (EPM) simplifies the modelling procedure of an AlGaN/GaN HEMT. By replacing both depletion charge layer and interface fixed charge layer by an equivalent voltage at passivation surface, depletion region can be modelled as a neutral region. Hence, Poisson equation can degenerate into Laplace equation [39].

In this paper, for an AlGaN/GaN HEMT with a p-layer in the barrier [42], an analytical model for the channel potential and electric field distributions is obtained. Under two assumptions of strong depletion (all the region between the gate edge of the source side and the drain region is depleted) and weak depletion (the region under the gate and the p-layer is depleted), the 2D Laplace equation with appropriate boundary conditions is solved.

The new electric field peak introduced by the p-layer is confirmed by the analytical model, which convincingly illustrates the electric field modification. The high electric field peak near the gate edge is efficiently reduced, and the electric field is more uniformly redistributed from the gate to the drain drift regions. As a consequence, breakdown voltage (BV) is improved from 90 V for the conventional AlGaN/GaN HEMTs (Con-HEMT) to 190 V for AlGaN/GaN HEMT with p-layer (p-HEMT). In addition, the variations of channel potential and electric field distributions with p-layer length (L_p) and thickness (T_p) are analysed. analytical model results are consistent with the simulated results using Silvaco software.

2. Device structure and analytical model

The schematic cross sectional view of AlGaN/GaN HEMT with a p-layer in the barrier layer is shown in Fig. 1, where x measures the horizontal position relative to the left edge of the gate while y measures the vertical position relative to the AlGaN layer. The epitaxial structure consists of a Si_3N_4 passivation layer, an AlGaN barrier layer, and GaN channel layer. We express the thicknesses of AlGaN, GaN and Si_3N_4 layers as d_1, d_2, and d_3 respectively. The dielectric constant of the AlGaN, GaN and Si_3N_4 layers are $\varepsilon_1=\varepsilon_0\varepsilon_{r1}$, $\varepsilon_2=\varepsilon_0\varepsilon_{r2}$ and $\varepsilon_3=\varepsilon_0\varepsilon_{r3}$, with ε_{r1}, ε_{r2} and ε_{r3} being the relative dielectric constant of AlGaN, GaN and Si_3N_4, respectively and ε_0 the vacuum permittivity. In this paper, m is used to express the molar fraction of Al in the AlGaN barrier layer. The dimensions of the device and symbols used in our model are listed in Table I. The L_1 represents the gate length; L_2-L_1denotes the length of the p-layer in the AlGaN barrier layer; L_3 indicates the distance from the gate edge near the source to the boundary of depletion region obtained from numerical results. The N_1, N_2 are the donor concentrations in the AlGaN barrier layer and the GaN channel layer, and σ_p is the polarization charge density.

The physical models Shockley-Read-Hall for recombination, impact ionization for generation, high field dependent mobility models, polarization model and Fermi-Dirac model are used in simulations with Silvaco software. The V_{DS} and V_{GS} are the bias voltages of the drain and gate, respectively. The device is biased in off-state to analyse the E-field distribution and potential distribution. The E-field in the source-side gate edge to the source region is negligible.

Hence, the AlGaN/GaN HEMT is divided into six regions, from the source-side gate edge to the depletion region boundary, which are denoted as I, II, III, IV, V, VI. The boundaries of the six regions are located at x=0, L_1, L_2, L_3, y=0, d_1, d_1+d_2, respectively.

Table I. symbols definition in analytical model and values in TCAD simulation.

Symbol	Definition	Value	Unit
L_S	source length	0.5	µm
L_G	gate length	0.5	µm
L_D	Drain length	0.5	µm
L_{GS}	Gate to source distance	1	µm
L_{GD}	Gate to drain distance	1.5	µm
L_P	p-layer length	0.4, 0.8 and 1	µm
T_p	p-layer thickness	5, 10 and 15	nm
d_1	AlGaN barrier thickness	22	nm
d_2	GaN channel thickness	0.25	µm
d_3	Si_3N_4 passivation layer thickness	10	nm
ε_0	Vacuum dielectric constant	8.8×10^{-12}	F/m
ε_{r1}	AlGaN relative dielectric constant	8.87	
ε_{r2}	GaN relative dielectric constant	8.9	
ε_{r3}	Si_3N_4 relative dielectric constant	7.5	
N_1	doping density of AlGaN layer	2×10^{18}	cm^{-3}
N_2	Background doping density of GaN	1×10^{15}	cm^{-3}
m	aluminium mole fraction of $Al_mGa_{1-m}N$	0.3	

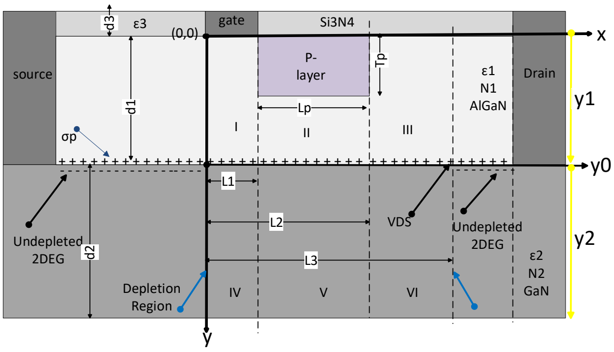

Fig.1. Schematic cross section of AlGaN/GaN HEMT with p-layer

When the device is biased in off-state, the charge in the depletion region can be classified into three parts: ionized donors fixed positive charge in AlGaN layer, interface fixed positive polarization charge along heterojunction interface in AlGaN layer and ionized fixed positive charges in GaN layer. Charge in the depletion region can be divided into differential charge layers of y_0, dy_1 and dy_2, respectively ($y_0=d_1$, $0<y_1<d_1$ and $d_1<y_2<d_1+d_2$). We defined the y_1 and y_2 axes to obtain the capacitors $C(y_1)$ and $C(y_2)$.

The doping profile in every layer is uniform, so the doping concentration $N(y_1)$, $N(y_2)$ can be denoted as N_1, N_2 respectively. Hence, the charge quantity of differential charge layers obtains as $dQ_0(y_0) = q\sigma_p$, $dQ_1(y_1) = q\,N(y_1)\,dy_1$, $dQ_2(y_2) = q\,N(y_2)\,dy_2$, σ_p (Polarization charge density at the interface of AlGaN/GaN). y_0 is an inherent differential charge layer introduced to model the polarization effect. The polarization effect of an AlGaN layer grown on a GaN buffer induces positive polarization charge at the AlGaN/GaN interface and negative polarization charge at the top of the AlGaN layer. Thus, an electric field is formed within the AlGaN layer. It is reasonable to regard the AlGaN surface and the AlGaN/GaN interface as two charged planes, in other words, the negative polarization charge at the top of the AlGaN layer and the positive polarization charge at the interface forms a planar plate capacitor, which generates no electric field outside its planes. Similarly, the GaN part, together with its counterpart at the bottom of the GaN layer, generates a uniform electric field pointing from the bottom of the GaN layer toward the AlGaN/GaN interface. Under the force of the electric field, conducting electrons (note that the AlGaN layer is n-doped) in AlGaN move to the channel, and form 2DEG in the channel [46]. Therefore differential charge layers and passivation layer surface can be evaluated as plates of differential capacitances [39]. The value of the differential capacitance in region I can be evaluated as capacitance of different layers connected in series yielding as:

$$C(y_0)=\left(\frac{d_1}{\varepsilon_1}\right)^{-1}\quad C(y_1)=\left(\frac{y_1}{\varepsilon_1}\right)^{-1}\quad C(y_2)=\left(\frac{d_1}{\varepsilon_1}+\frac{y_2}{\varepsilon_2}\right)^{-1} \tag{1}$$

The value of the differential capacitance in regions II and III are:

$$C(y_0)=\left(\frac{d_1}{\varepsilon_1}+\frac{d_3}{\varepsilon_3}\right)^{-1}\qquad C(y_1)=\left(\frac{y_1}{\varepsilon_1}+\frac{d_3}{\varepsilon_3}\right)^{-1}$$

$$C(y_2)=\left(\frac{d_1}{\varepsilon_1}+\frac{d_3}{\varepsilon_3}+\frac{y_2}{\varepsilon_2}\right)^{-1} \tag{2}$$

By using parallel plate capacitance theory, the differential charge layers can be equivalent to the differential potential applied at passivation layer surface. Since the differential equivalent potential has been derived by $dv=\frac{dQ}{C}$, the total equivalent potential at passivation layer surface can be obtained by integrating the differential equivalent potential. In region I:

$$V_{01}=\frac{dQ_0(y_0)}{C(y_0)}=q\sigma_p\left(\frac{d_1}{\varepsilon_1}\right) \tag{3}$$

$$V_{11}=\int_0^{d_1}qN_1(y_1)\left(\frac{y_1}{\varepsilon_1}\right)dy_1=qN_1\left(\frac{(d_1)^2}{2\varepsilon_1}\right) \tag{4}$$

$$V_{21}=-\int_{d_1}^{d_1+d_2}qN_2(y_2)\left(\frac{d_1}{\varepsilon_1}+\frac{y_2}{\varepsilon_2}\right)dy_2=-qN_2\left(\frac{d_1d_2}{\varepsilon_1}+\frac{(d_2)^2+2d_1d_2}{2\varepsilon_2}\right) \tag{5}$$

$$V_{equ1}=V_{01}+V_{11}+V_{21} \tag{6}$$

In region II:

$$V_{02}=q\sigma_p\left(\frac{d_1}{\varepsilon_1}+\frac{d_3}{\varepsilon_3}\right) \tag{7}$$

$$V_{12}=\int_{T_p}^{d_1}qN_1(y_1)\left(\frac{y_1}{\varepsilon_1}+\frac{d_3}{\varepsilon_3}\right)dy_1=qN_1\left(\frac{(d_1)^2-(T_p)^2}{2\varepsilon_1}+\frac{d_3(d_1-T_p)}{\varepsilon_3}\right) \tag{8}$$

$$V_{22}=-\int_{d_1}^{d_1+d_2}qN_2(y_2)\left(\frac{d_1}{\varepsilon_1}+\frac{y_2}{\varepsilon_2}+\frac{d_3}{\varepsilon_3}\right)dy_2=-qN_2\left(\frac{d_1d_2}{\varepsilon_1}+\frac{(d_2)^2+2d_1d_2}{2\varepsilon_2}+\frac{d_3d_2}{\varepsilon_3}\right) \tag{9}$$

$$V_{equ2}=V_{02}+V_{12}+V_{22} \tag{10}$$

In region III:

$$V_{03}=V_{02} \tag{11}$$

$$V_{13}=\int_0^{d_1}qN_1(y_1)\left(\frac{y_1}{\varepsilon_1}+\frac{d_3}{\varepsilon_3}\right)dy_1=qN_1\left(\frac{(d_1)^2}{2\varepsilon_1}+\frac{d_3d_1}{\varepsilon_3}\right) \tag{12}$$

$$V_{23}=V_{22} \tag{13}$$

$$V_{equ3}=V_{03}+V_{13}+V_{23} \tag{14}$$

Thus, through EPM, all charges in depletion region are transferred to the potential at passivation layer surface which can be utilized as boundary conditions for modelling, therefor six 2D potential functions are introduced to describe the potential distribution in six regions shown in Fig.1. which are $\phi_{11}(x, y)$ (in region I for $0 \le x \le L_1$, $0 \le y \le d_1$), $\phi_{12}(x, y)$ (in region II for $L_1 \le x \le L_2$, $0 \le y \le d_1$), $\phi_{13}(x, y)$ (in region III for $L_2 \le x \le L_3$, $0 \le y \le d_1$), $\phi_{21}(x, y)$ (in region IV for $0 \le x \le L_1$, $d_1 \le y \le d_1+d_2$), $\phi_{22}(x, y)$ (in region V for $L_1 \le x \le L_2$, $d_1 \le y \le d_1+d_2$), $\phi_{23}(x, y)$ (in region VI for $L_2 \le x \le L_3$, $d_1 \le y \le d_1+d_2$) respectively. By using EPM, the depletion region can be assumed as neutral, thus Poisson equations can be degenerated into Laplace equations ((15) in Appendix) [34].

The potential function ϕ_{ij} (x, y) in the vertical direction can be approximated by a simple parabolic function [43] that is shown in the Appendix with relation (16). In this relation, the potential at the heterojunction interface is $\phi_j(x)= \phi_{1j}(x, d_1) = \phi_{2j}(x, d_1)$. b_{ij} and c_{ij} are the unknown coefficients, which need to be solved [40].

The Laplace equations (15) are solved using the following boundary conditions. Heterojunction potential at the right boundary of region III is assumed to be V_{DS} and the left boundary of region I can be evaluated as V_{bi} as shown in Appendix, where V_{bi} is built in voltages [36].

The potentials at the AlGaN/GaN interface are continuous in vertical direction ((19)-(21) in Appendix) [35].

Electric displacement at the AlGaN/GaN interface is continuous ((22)-(24) in Appendix), so by EPM the depletion region can be as a neutral region and consequently the charge quantity at the heterojunction interface is eliminated [34].

Electric field at the bottom of GaN layer minimized ((25) in Appendix) [41]. Which is due to the fact that the thickness of GaN layer d_2 is large enough, i.e. d_2=0.2 µm.

Electric displacement at the interface between the passivation layer and AlGaN layer is continuous [34, 39].

for $j=2,3$

$$-\varepsilon_1 \frac{\partial \varphi_{1j}(x,y)}{\partial y} \Big|_{y=0} = \varepsilon_3 \frac{V_f(x)+V_{equj}-\varphi_{1j}(x,0)}{d_3} \quad (26)$$

$V_f(x)$ is the potential at the surface of Si_3N_4 passivation layer. Two approximations were used for $V_f(x)$ in regions II and III (L_1 <x<L_3) [37-39].

1. For a strong depletion, $V_{f1}(x)$ in regions II and III (L_1 <x<L_3) linearly increases from V_{GS} to V_{DS} ((27) in Appendix).
2. For a weak depletion, $V_{f2}(x)$ in regions II and III (L_1 <x<L_3) is given by (28) in Appendix.

In general, $V_f(x)$ ((29) in Appendix) can be modeled as the combination of $V_{f1}(x)$ and $V_{f2}(x)$ by a coefficient η determined by the V_{DS} and device structure parameters, for η=0 weak depletion, η=1 strong depletion and 0<η<1 between two depletion modes [39].

Potential at the interface between the gate and the AlGaN layer is

$$\varphi_{11}(x,0) = V_{GS} - V_{FB} + V_{equ1} = V_g \quad (30)$$

V_{FB} is the flat band voltage, $V_{FB}=\varphi_{MS}=\varphi_M-\varphi_s$, φ_M is the metal gate work function and the semiconductor ($Al_mGa_{1-m}N$) work function φ_s is given by (31) in the Appendix [43]. Where E_g is the $Al_mGa_{1-m}N$ band gap, χ_d is the electron affinity of $Al_mGa_{1-m}N$, $\varphi_f=(KT/q)\ln(N_c/N_1)$, K is the Boltzmann constant, N_c is the effective density of states in conduction band in AlGaN layer and T=300 K.

The electric field and potential continuity at the interface of each region in the AlGaN layer and the GaN layer represented as (32) and (33) in the Appendix [41].

The polarization charge density σ_p is determined by the Al composition in the AlGaN material and the thickness of the AlGaN layer. Based on the polarization theories [36, 37], σ_p at the AlGaN/GaN heterojunction interface in AlGaN layer due to the piezoelectric and spontaneous polarizations are given by (34) in the Appendix [36, 37]. Where $P_{SP}(Al_mGa_{1-m}N) - P_{SP}(GaN)$, is the interface charge due to the spontaneous polarization at AlGaN/GaN heterostructure, and P_{PE} is the interface charge due to the variation of the strain induced piezoelectric polarization ((35) in the Appendix) at AlGaN/GaN heterostructure, r(m) is the degree of strain relaxation of the $Al_mGa_{1-m}N$ layer, a_{GaN} and $a_{AlGaN}(m)$ are the crystal lattice constants for GaN and $Al_mGa_{1-m}N$, respectively; $c_{13}(m)$ and c_{33} (m) are the elastic constants; $e_{31}(m)$ and $e_{33}(m)$ are the piezoelectric constants. All the parameters in Eqs. (34) and (35) can be found in Ref. [36].

Substituting Eq. (16) into Eq. (15) yields

$$\frac{\partial^2 \varphi_j(x)}{\partial x^2} + 2c_{ij} = 0 \quad i=1,2 \quad j=1,2,3 \quad (36)$$

According to the boundary conditions (19)-(31), the coefficient c_{ij} (i=1, 2 j=1, 2, 3) could be represented by $\varphi_j(x)$ and therefore equation (36) could be simplified into

$$\frac{\partial^2 \varphi_1(x)}{\partial x^2} - \frac{\varphi_1(x)}{t_1^2} = -\frac{V_g}{t_1^2} \quad (37)$$

$$\frac{\partial^2 \varphi_2(x)}{\partial x^2} - \frac{\varphi_2(x)}{t_2^2} = -\frac{V_f(x)+V_{equ2}}{t_2^2} \quad (38)$$

$$\frac{\partial^2 \varphi_3(x)}{\partial x^2} - \frac{\varphi_3(x)}{t_3^2} = -\frac{V_f(x)+V_{equ3}}{t_3^2} \quad (39)$$

The specific parameters are shown below (40)-(41)

$$t_1 = (\frac{d_1^2}{2} + \frac{d_1 d_2 \varepsilon_2}{\varepsilon_1})^{\frac{1}{2}} \quad (40)$$

$$t_2 = t_3 = t = (\frac{d_1^2}{2} + \frac{\varepsilon_1 d_1 d_3}{\varepsilon_3} + \frac{d_1 d_2 \varepsilon_2}{\varepsilon_1} + \frac{\varepsilon_2 d_2 d_3}{\varepsilon_3})^{\frac{1}{2}} \quad (41)$$

Based on the above equations, the potential at the heterojunction interface is $\phi_j(x)=\phi_{1j}(x)=\phi_{2j}(x)$ (j=1,2,3).

$$\varphi_{11}(x,d_1) = A_1 \sinh\left(\frac{x}{t_1}\right) + A_2 \sinh\left(\frac{L_1-x}{t_1}\right) + V_g \quad 0<x<L_1 \quad (42)$$

$$\varphi_{12}(x,d_1) = B_1 \sinh(\frac{x-L_1}{t}) + B_2 \sinh(\frac{L_2-x}{t}) + V_{equ2} + V_{f1}(x) \quad L_1<x<L_2 \quad (43)$$

$$\varphi_{13}(x,d_1) = C_1 \sinh(\frac{x-L_2}{t}) + C_2 \sinh(\frac{L_3-x}{t}) + V_{equ3} + V_{f1}(x) \quad L_2<x<L_3 \quad (44)$$

$$\varphi_{21}(x,d_1) = D_1 \sinh\left(\frac{x}{t_1}\right) + D_2 \sinh\left(\frac{L_1-x}{t_1}\right) + V_g \quad 0<x<L_1 \quad (45)$$

$$\varphi_{22}(x,d_1) = E_1 \sinh(\frac{x-L_1}{t}) + E_2 \sinh(\frac{L_2-x}{t}) + V_{equ2} + V_{f2}(x) \quad L_1<x<L_2 \quad (46)$$

$$\varphi_{23}(x,d_1) = F_1 \sinh(\frac{x-L_2}{t}) + F_2 \sinh(\frac{L_3-x}{t}) + V_{equ3} + V_{f2}(x) \quad L_2<x<L_3 \quad (47)$$

By substituting (17-18), (32-33) into (42)-(47), coefficients can be computed and are shown in the Appendix, including a_1, b_1, c_1, d_1, e_1, f_1, g_1, A_1, A_2, B_1, B_2, C_1, C_2, D_1, D_2, E_1, E_2, F_1 and F_2.
therefore, the potential distribution along the heterointerface of AlGaN/GaN for the two depletion modes can be modeled by a linear combination of $\varphi_{1j}(x,d_1)$ and $\varphi_{2j}(x,d_1)$ as (48) [39].

$$\varphi_j(x) = \eta\varphi_{1j}(x,d_1) + (1-\eta)\varphi_{2j}(x,d_1) \quad j=1,2,3 \quad (48)$$

Where η is the weight factor and is determined to be 0.2 ~ 0.7.

$$\varphi_1(x) = (\eta A_1 + (1-\eta)D_1)\sinh(\frac{x}{t_1}) + (\eta A_2 + (1-\eta)D_2)\sinh(\frac{L_1-x}{t_1}) + V_g \quad 0<x<L_1 \quad (49)$$

$$\varphi_2(x) = (\eta B_1 + (1-\eta)E_1)\sinh(\frac{x-L_1}{t}) + (\eta B_2 + (1-\eta)E_2)\sinh(\frac{L_2-x}{t}) + V_{equ2} + \frac{\eta(V_{DS}-V_{GS})(x-L_3)}{L_3-L_1} + V_{DS} \quad L_1<x<L_2 \quad (50)$$

$$\varphi_3(x) = (\eta C_1 + (1-\eta)F_1)\sinh\left(\frac{x-L_2}{t}\right) + (\eta C_2 + (1-\eta)F_2)\sinh\left(\frac{L_3-x}{t}\right) + V_{equ3} + \frac{\eta(V_{DS}-V_{GS})(x-L_3)}{L_3-L_1} + V_{DS} \qquad L_2 < x < L_3 \tag{51}$$

The AlGaN/GaN heterostructure channel electric field $E_j(x)$ distribution can be obtained by differentiating potential distribution in (52)-(54).

$$E_1(x) = (\eta A_1 + (1-\eta)D_1)\frac{1}{t_1}\cosh\left(\frac{x}{t_1}\right) - (\eta A_2 + (1-\eta)D_2)\frac{1}{t_1}\cosh\left(\frac{L_1-x}{t_1}\right) \qquad 0 < x < L_1 \tag{52}$$

$$E_2(x) = (\eta B_1 + (1-\eta)E_1)\frac{1}{t}\cosh\left(\frac{x-L_1}{t}\right) - (\eta B_2 + (1-\eta)E_2)\frac{1}{t}\cosh\left(\frac{L_2-x}{t}\right) + \frac{\eta(V_{DS}-V_{GS})}{L_3-L_1} \qquad L_1 < x < L_2 \tag{53}$$

$$E_3(x) = (\eta C_1 + (1-\eta)F_1)\frac{1}{t}\cosh\left(\frac{x-L_2}{t}\right) - (\eta C_2 + (1-\eta)F_2)\frac{1}{t}\cosh\left(\frac{L_3-x}{t}\right) + \frac{\eta(V_{DS}-V_{GS})}{L_3-L_1} \qquad L_2 < x < L_3 \tag{54}$$

3. Results and discussion

Based on the above analytical model, the potential and the lateral electric field distributions along the AlGaN/GaN hetero-structure channel could be obtained. In order to verify the proposed model, the 2D device numerical simulations are performed using Silvaco-Atlas device simulator. In the simulated device structure, doping concentration of the p-layer is the same as the n-type doping in the barrier layer. Nickel is chosen for the gate Schottky contact with a work function 5.1 eV. In the following figures, the symbols with different shapes represent the analytical model results; whereas, the solid lines signify the simulation results.

Fig. 2 shows the comparison of the surface potential distribution and surface electric field of conventional AlGaN/GaN HEMT (Con-HEMT) and AlGaN/GaN HEMT with p-layer in the barrier (P-HEMT), respectively. The analytical model is in good agreement with the simulation results, and the validity of the model is verified.

For Con-HEMT, the high-density 2DEG at the heterojunction interface is uniformly distributed and cannot be completely depleted in the drift region. The depletion region is narrow (approximately 1.08 µm). therefore, the electric potential increases within the 1.08 µm spacing and remains unchanged. The highest electric field is on the drain side of the gate edge, and the electric field rapidly decreases along the drift region. For the p-HEMT, the 2DEG density near the gate edge reduces due to the p-layer in the barrier. The lower 2DEG concentration contributes to the depletion region extension. We observe that when T_p is 15 nm and L_p is 0.8 µm, the drift region is more depleted (approximately 1.4 µm). Therefore, the electric potential gradually increases within the 1.4 µm spacing along the depleted drift region and remains unchanged beyond 1.4 µm. Meanwhile, a new electric field peak is introduced by the p-layer. The presence of the new electric field peak effectively reduces the electric field peak at the drain side gate edge. Consequently, the electric field distribution becomes more uniform. BV of the device improves from 90 V for the Con-HEMT to 190 V for the p-HEMT with T_p=15 nm and L_p=0.8 µm. The surface electric field can be modified to improve the breakdown voltage by the electric field modulation based on changing the charge distribution inside the device [3].

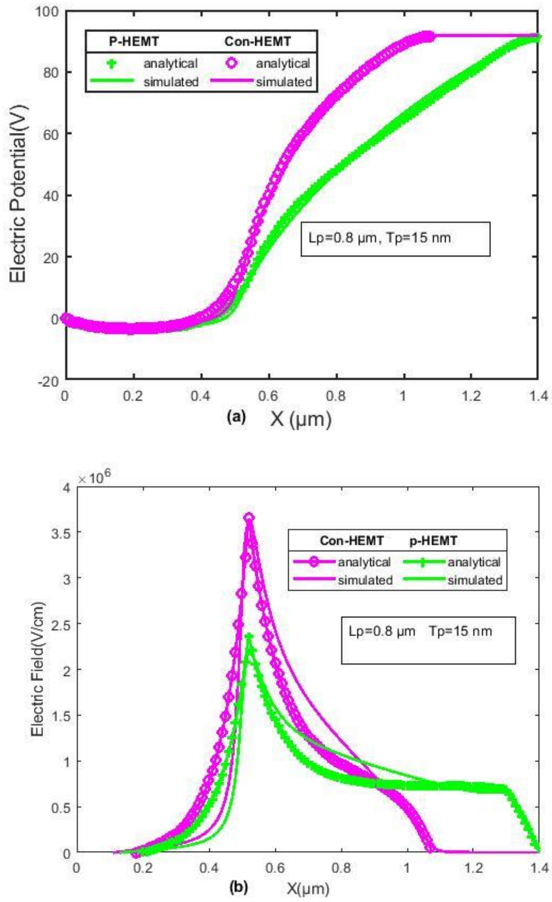

Fig.2. Comparison of P-HEMTs and Con-HEMTs. (a) Electric potential, (b) Electric field distributions.

The main parameters that affect BV of the AlGaN/GaN p-HEMT are T_p and L_p. At a fixed L_p of 0.8 µm, the 2DEG density decreases and tends to saturate when T_p increases. The depletion region is extended in the drift region at high V_{DS} voltages. Upon increasing T_p from 5nm to 10 nm and 15 nm, the drift region is more depleted. Hence, the electric potential smoothly increases along the depleted drift region. The maximum potential value increases with increasing T_p, as shown in Fig. 3 (a). In other words, device BV improves, i.e. the BV for the P-HEMT structure with T_p 5, 10, and 15 nm at a fixed L_p (0.8 µm) are about 110 V, 145 V and 190 V, respectively. Simultaneously, the new electric field peak that arises from the p-layer in the barrier increases. As shown in Fig. 3 (b) the high electric field peak near the gate edge is effectively reduced because the electric field modulation effect strengthens.

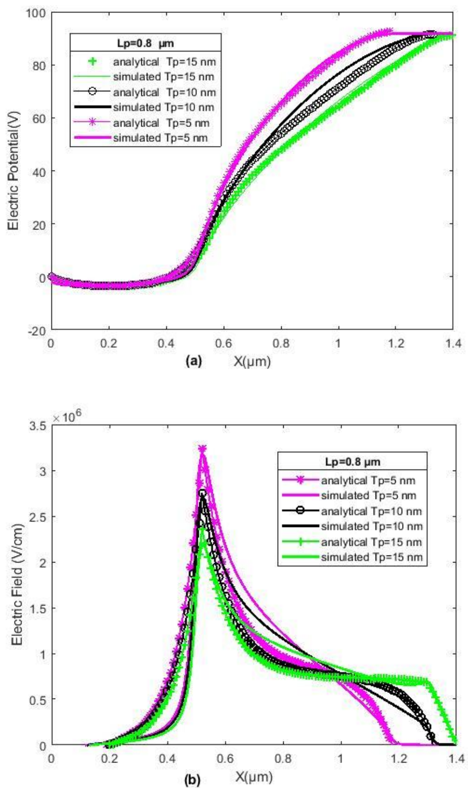

Fig.3. Electric potential (a), Electric field (b) of the P-HEMT with different TP

At a fixed T_p of 15 nm, with increasing L_p, the low-density 2DEG region and the depletion region lengths become longer. As shown in Fig. 4 (a), at L_p of 0.4, 0.8, and 1 µm, the drift region is incompletely depleted. Thus, the electric potential increases within depleted region and remain constant in region 2DEG.

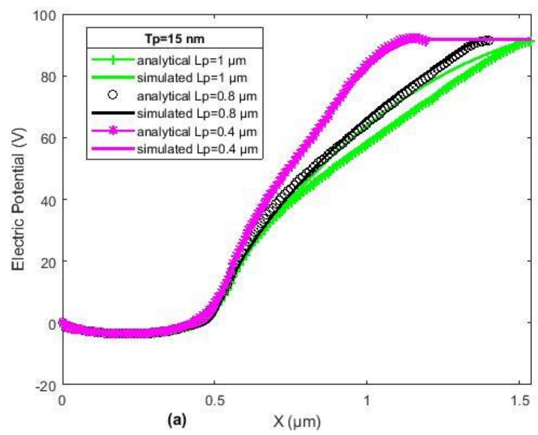

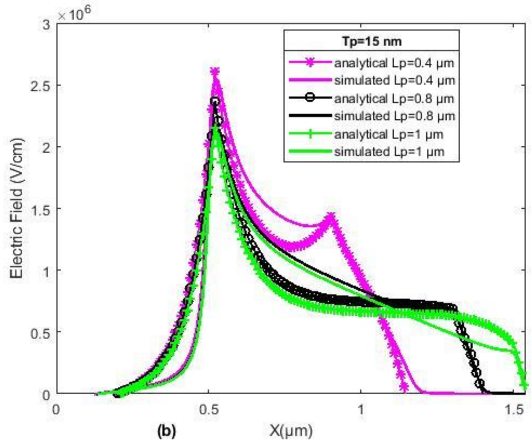

Fig.4. Electric potential distributions (a), Electric field distributions (b) of the P-HEMT with different Lp

The new electric field peak, which results from the p-layer in the barrier, increases and shifts toward the drain electrode, which causes the high electric field peak near the gate edge on the drain side to decrease and consequently, the BV to increase. The BV of the P-HEMT structure with L_p 0.4, 0.8, and 1 µm at a fixed T_p (15 nm) are about 150 V, 190 V and 210 V, respectively.

4. Conclusions

In this paper, a 2D analytical model for the channel potential and electric field distributions of AlGaN/GaN HEMT with a p-layer in the barrier is presented. The effect of various p-layer thicknesses and lengths on the channel potential and electric field distributions are discussed in detail. When the p-layer thickness and length increase, potential distribution is modified which reduces the high electric field peak near the drain side of the gate edge and therefore increases BV. The BV of the device improves from 90 V for the Con-HEMT to 190 V for the HEMT with L_p=0.8 µm and T_p=15 nm. The accuracy of the analytical model is verified in comparison with the simulated results. A fair consistency between the analytical and numerical results indicates the validity of the proposed analytical model. The method can be employed to develop other analytical models for different device structures, such as FP-HEMT, HEMT with GaN cap layer, HEMT with etch in the barrier or channel and HEMT with undoped region in the barrier with a little change in boundary conditions.

5. Appendix

$$\frac{\partial^2\varphi_{ij}(x,y)}{\partial x^2}+\frac{\partial^2\varphi_{ij}(x,y)}{\partial y^2}=0 \quad i=1,2,\ j=1,2,3 \tag{15}$$

$$\varphi_{ij}(x,y)=\varphi_j(\mathrm{x})+b_{ij}(\mathrm{y}-d_1)+c_{ij}(y-d_1)^2 \quad i=1,2, \quad j=1,2,3 \tag{16}$$

$$\varphi_{11}\,(0,d_1)=V_{bi} \tag{17}$$

$$\varphi_{13}\,(L_3,d_1)=V_{DS}+V_{bi} \tag{18}$$

$$\varphi_{11}(\mathrm{x}, d_1) = \varphi_{21}(\mathrm{x}, d_1) \quad (19)$$
$$\varphi_{12}(\mathrm{x}, d_1) = \varphi_{22}(\mathrm{x}, d_1) \quad (20)$$
$$\varphi_{13}(\mathrm{x}, d_1) = \varphi_{23}(\mathrm{x}, d_1) \quad (21)$$

$$-\varepsilon_1 \frac{\partial \varphi_{11}(x,y)}{\partial y}\Big|_{y=d_1} = -\varepsilon_2 \frac{\partial \varphi_{21}(x,y)}{\partial y}\Big|_{y=d_1} \quad (22)$$
$$-\varepsilon_1 \frac{\partial \varphi_{12}(x,y)}{\partial y}\Big|_{y=d_1} = -\varepsilon_2 \frac{\partial \varphi_{22}(x,y)}{\partial y}\Big|_{y=d_1} \quad (23)$$
$$-\varepsilon_1 \frac{\partial \varphi_{13}(x,y)}{\partial y}\Big|_{y=d_1} = -\varepsilon_2 \frac{\partial \varphi_{23}(x,y)}{\partial y}\Big|_{y=d_1} \quad (24)$$

$$\frac{\partial \varphi_{2j}(x,y)}{\partial y}\Big|_{y=d_1+d_2} = 0 \qquad j = 1,2,3 \quad (25)$$

$$V_{f1}(x) = \frac{(V_{DS}-V_{GS})(x-L_1)}{(L_3-L_1)} + V_{GS} \quad (27)$$
$$V_{f2}(x) = V_{DS} \quad (28)$$
$$V_f(x) = \eta\, V_{f1}(x) + (1-\eta)\, V_{f2}(x) \quad (29)$$

$$\phi_s = \chi_d + \frac{E_g}{2} - \phi_f \quad (31)$$

$$\varphi_{11}(L_1, d_1) = \varphi_{12}(L_1, d_1), \qquad \frac{\partial \varphi_{11}(x,d_1)}{\partial x}\Big|_{x=L_1} = \frac{\partial \varphi_{12}(x,d_1)}{\partial x}\Big|_{x=L_1} \quad (32)$$
$$\varphi_{12}(L_2, d_1) = \varphi_{13}(L_2, d_1), \qquad \frac{\partial \varphi_{12}(x,d_1)}{\partial x}\Big|_{x=L_2} = \frac{\partial \varphi_{13}(x,d_1)}{\partial x}\Big|_{x=L_2} \quad (33)$$

$$\sigma_p(m) = |P_{PE}(Al_mGa_{1-m}N) + P_{SP}(Al_mGa_{1-m}N) - P_{SP}(GaN)| \quad (34)$$

$$P_{PE}(Al_mGa_{1-m}N) = 2[1-r(m)]\frac{a_{GaN}-a_{AlGaN}(m)}{a_{AlGaN}(m)} \times \left[e_{31}(m) - e_{33}(m)\frac{c_{13}(m)}{c_{33}(m)}\right] \quad (35)$$

$$a_1 = \frac{1}{t_1}\cosh\left(\frac{L_1}{t_1}\right) + \frac{1}{t}\coth\left(\frac{L_2-L_1}{t}\right)\sinh\left(\frac{L_1}{t_1}\right) \quad (55)$$

$$b_1 = \frac{-V_g}{t_1 sinh\frac{L_1}{t_1}} - \frac{1}{t}coth\left(\frac{L_2-L_1}{t}\right)\left[V_g - V_{equ2} - V_{GS}\right] + \frac{V_{DS}-V_{GS}}{L_3-L_1} \quad (56)$$

$$c_1 = cosh\left(\frac{L_2-L_1}{t}\right) + coth\left(\frac{L_3-L_2}{t}\right)sinh\left(\frac{L_2-L_1}{t}\right) \quad (57)$$

$$d_1 = \frac{-V_{equ3}}{sinh\left(\frac{L_3-L_2}{t}\right)} + \frac{V_g-V_{equ2}-V_{GS}}{sinh\left(\frac{L_2-L_1}{t}\right)} - coth\left(\frac{L_3-L_2}{t}\right)(V_{equ2} - V_{equ3}) \quad (58)$$

$$A_1 = \frac{b_1c_1+\frac{1}{t}d_1}{a_1c_1 - \frac{sinh\left(\frac{L_1}{t_1}\right)}{tsinh\left(\frac{L_2-L_1}{t}\right)}} \qquad A_2 = \frac{-V_g}{sinh\left(\frac{L_1}{t_1}\right)} \quad (59)$$

$$B_1 = \frac{a_1d_1 + \frac{b_1\sinh\left(\frac{L_1}{t_1}\right)}{\sinh\left(\frac{L_2-L_1}{t}\right)}}{a_1c_1 - \frac{\sinh\left(\frac{L_1}{t_1}\right)}{tsinh\left(\frac{L_2-L_1}{t}\right)}} \qquad B_2 = \frac{A_1\sinh\left(\frac{L_1}{t_1}\right)}{\sinh\left(\frac{L_2-L_1}{t}\right)} + \frac{V_g-V_{equ2}-V_{GS}}{\sinh\left(\frac{L_2-L_1}{t}\right)} \quad (60)$$

$$C_1 = \frac{-V_{equ3}}{\sinh\left(\frac{L_3-L_2}{t}\right)} \quad C_2 = \frac{B_1\sinh\left(\frac{L_2-L_1}{t}\right)}{\sinh\left(\frac{L_3-L_2}{t}\right)} + \frac{V_{equ2}-V_{equ3}}{\sinh\left(\frac{L_3-L_2}{t}\right)} \quad (61)$$

$$e_1 = \frac{-V_g}{t_1\sinh\left(\frac{L_1}{t_1}\right)} - \frac{1}{t}\coth\left(\frac{L_2-L_1}{t}\right)(V_g - V_{equ2} - V_{DS}) \quad (62)$$

$$f_1 = \cosh\left(\frac{L_2-L_1}{t}\right) + \coth\left(\frac{L_3-L_2}{t}\right)\sinh\left(\frac{L_2-L_1}{t}\right) \quad (63)$$

$$g_1 = \frac{-V_{equ3}}{\sinh\left(\frac{L_3-L_2}{t}\right)} + \frac{V_g-V_{equ2}-V_{DS}}{\sinh\left(\frac{L_2-L_1}{t}\right)} - \coth\frac{L_3-L_2}{t}\left(V_{equ2} - V_{equ3}\right) \quad (64)$$

$$D_1 = \frac{e_1f_1+\frac{g_1}{t}}{a_1f_1 - \frac{\sinh\left(\frac{L_1}{t_1}\right)}{tsinh\left(\frac{L_2-L_1}{t}\right)}} \qquad D_2 = \frac{-V_g}{\sinh\left(\frac{L_1}{t_1}\right)} \quad (65)$$

$$E_1 = \frac{a_1g_1 + \frac{e_1\sinh\left(\frac{L_1}{t_1}\right)}{\sinh\left(\frac{L_2-L_1}{t}\right)}}{a_1f_1 - \frac{\sinh\left(\frac{L_1}{t_1}\right)}{tsinh\left(\frac{L_2-L_1}{t}\right)}} \qquad E_2 = \frac{D_1\sinh\left(\frac{L_1}{t_1}\right)}{\sinh\left(\frac{L_2-L_1}{t}\right)} + \frac{V_g-V_{equ2}-V_{DS}}{\sinh\left(\frac{L_2-L_1}{t}\right)} \quad (66)$$

$$F_1 = \frac{-V_{equ3}}{\sinh\left(\frac{L_3-L_2}{t}\right)} \qquad F_2 = \frac{E_1\sinh\left(\frac{L_2-L_1}{t}\right)}{\sinh\left(\frac{L_3-L_2}{t}\right)} + \frac{V_{equ2}-V_{equ3}}{\sinh\left(\frac{L_3-L_2}{t}\right)} \quad (67)$$

6. References

[1] M.T.B. Kashem, S. Subrina, "Analytical modeling of channel potential and threshold voltage of triple material gate AlGaN/GaN HEMT including trapped and polarization-induced charges". *International Journal of Numerical Modelling: Electronic Networks, Devices and Fields*, vol. 32, no. 1, pp. e2476-e2490, 2019.

[2] S. Zhu, H. Jia, T. Li, Y. Tong, Y. Liang, X. Wang, T. Zeng, Y. Yang, "Novel high-energy-efficiency AlGaN/GaN HEMT with high gate and multi-recessed buffer". *Micromachines*, vol. 10, no. 7, pp. 444-456, 2019.

[3] L. Yang, B. Duan, Z. Dong, Y. Wang, Y. Yang, "The analysis model of AlGaN/GaN HEMTs with electric field modulation effect", *IETE Technical Review*, vol. 37, no. 6, pp. 553-564, 2020.

[4] F. Bernardini, V. Fiorentini, D. Vanderbilt, "Spontaneous polarization and piezoelectric constants of III-V nitrides", *Physical Review B*, vol. 56, no.16, pp. R10024- R10027, 1997.

[5] E.S.Hellman, "The polarity of GaN: a critical review", *Materials Research Society Internet Journal of Nitride Semiconductor Research*, vol. 3, pp. e11-e22, 1998.

[6] O. Ambacher, J. Smart, J.R. Shealy, N.G. Weimann, K. Chu, M. Murphy, W.J. Schaff, L.F. Eastman, "Two-dimensional electron gases induced by spontaneous and piezoelectric polarization charges in N-and Ga-face AlGaN/GaN heterostructures". *Journal of applied physics*, vol. 85, no.6, pp. 3222-3233, 1999.

[7] O. Ambacher, B. Foutz, J. Smart, J.R. Shealy, N.G. Weimann, K. Chu, M. Murphy, A.J. Sierakowski, W.J. Schaff, and L.F. Eastman, "Two-dimensional electron gases induced by spontaneous and piezoelectric polarization in undoped and doped AlGaN/GaN heterostructures", *Journal of applied physics*, vol. 87, no.1, pp. 334-344, 2000.

[8] J.P. Ibbetson, P.T. Fini, K.D. Ness, S.P. DenBaars, J.S. Speck, and U.K. Mishra, "Polarization effects, surface states, and the source of electrons in AlGaN/GaN

heterostructure field effect transistors", *Applied Physics Letters*, vol. 77, no.2, pp. 250-252, 2000.

[9] O. Ambacher, J. Majewski, C. Miskys, A. Link, M. Hermann, M. Eickhoff, M. Stutzmann, F. Bernardini, V. Fiorentini, V. Tilak, B. Schaff, L.F. Eastman, "Pyroelectric properties of Al (In) GaN/GaN hetero-and quantum well structures", Journal of physics: condensed matter, vol. 14, no.13, pp. 3399-3434, 2002.

[10] S. Heikman, S. Keller, Y. Wu, J.S. Speck, S.P. DenBaars, U.K. Mishra, "Polarization effects in AlGaN/GaN and GaN/AlGaN/GaN heterostructures", *Journal of applied physics*, vol. 93, no.12, pp. 10114-10118, 2003.

[11] S. Karmalkar, U.K. Mishra, "Enhancement of breakdown voltage in AlGaN/GaN high electron mobility transistors using a field plate", *IEEE transactions on electron devices*, vol. 48, no.8, pp. 1515-1521, 2001.

[12] S. Karmalkar, M.S. Shur, G. Simin, M.A. Khan, "Field-plate engineering for HFETs", *IEEE Transactions on electron devices*, vol. 52, no.12, pp. 2534-2540, 2005.

[13] Y. Dora, A. Chakraborty, L. McCarthy, S. Keller, S.P. DenBaars, U.K. Mishra, "High breakdown voltage achieved on AlGaN/GaN HEMTs with integrated slant field plates", *IEEE Electron Device Letters*, vol. 27, no.9, pp. 713-715, 2006.

[14] Y.-F. Wu, M. Moore, A. Saxler, T. Wisleder, P. Parikh, "40-W/mm double field-plated GaN HEMTs", In 2006 64th device research conference, IEEE, June 2006, State College, PA, USA, pp. 151-152.

[15] Y. Pei, Z. Chen, D. Brown, S. Keller, S. P. Denbaars, U. K. Mishra, "Deep-submicrometer AlGaN/GaN HEMTs with slant field plates", *IEEE electron device letters*, vol. 30, no.4, pp. 328-330, 2009.

[16] E.B. Treidel, O. Hilt, F. Brunner, V. Sidorov, J. Würfl, G. Tränkle, "AlGaN/GaN/AlGaN DH-HEMTs breakdown voltage enhancement using multiple grating field plates (MGFPs)", *IEEE Transactions on Electron Devices*, vol. 57, no.6, pp. 1208-1216, 2010.

[17] K.-H. Cho, Y.-S. Kim, J. Lim, Y.-H. Choi, M.-K. Han, "Design of AlGaN/GaN HEMTs employing mesa field plate for breakdown voltage enhancement", *Solid-state electronics*, vol. 54, no.4, pp. 405-409, 2010.

[18] T. Asano, N. Yamada, T. Saito, H. Tokuda, M. Kuzuhara, "Breakdown characteristics in AlGaN/GaN HEMTs with multi-field-plate structure" in 2012 IEEE International Meeting for Future of Electron Devices Kansai, IEEE, May 2012, Suita, Japan.

[19] T. Deguchi, A. Kamada, M. Yamashita, H. Tomita, M. Arai, K. Yamasaki, T. Egawa, "High-voltage AlGaN/GaN HFETs by using graded gate field plates", *Electronics letters*, vol. 48, no.2, pp. 109-110, 2012.

[20] G. Xie, E. Xu, J. Lee, N. Hashemi, B. Zhang, F.Y. Fu, W.T. Ng, "Breakdown-voltage-enhancement technique for RF-based AlGaN/GaN HEMTs with a source-connected air-bridge field plate", *IEEE electron device letters*, vol. 33, no.5, pp. 670-672, 2012.

[21] K. Jena, R. Swain, T.R. Lenka, "Impact of a drain field plate on the breakdown characteristics of AlInN/GaN MOSHEMT", *Journal of the Korean Physical Society*, vol. 67, no.9, pp. 1592-1596, 2015.

[22] A. Soni, Ajay, M. Shrivastava "Novel drain-connected field plate GaN HEMT designs for improved V BD–R ON tradeoff and RF PA performance", *IEEE Transactions on Electron Devices*, vol. 67, no.4, pp. 1718-1725, 2020.

[23] K.-H. Cho, Y.-H. Choi, J. Lim, M.-K. Han, "Increase of breakdown voltage on AlGaN/GaN HEMTs by employing proton implantation", *IEEE transactions on electron devices,* vol. 56, no.3, pp. 365-369, 2009.

[24] B. Duan, Y.T. Yang, "Breakdown voltage analysis for the new RESURF AlGaN/GaN HEMTs", *Science China Information Sciences*, vol. 55, no.2, pp. 473-479, 2012.

[25] B. Duan, Y. Yang, "New $Al_{0.25}Ga_{0.75}N$/GaN HEMTs structure with the partial silicon doping", *Micro & Nano Letters*, vol. 7, no.1, pp. 9-11, 2012.

[26] H. Guo, B. Duan, S. Xie, S. Yuan, Y. Yang, "Enhancement-mode AlGaN/GaN HEMTs with optimized electric field using a partial GaN cap layer", *Micro & Nano Letters*, vol. 12, no.10, pp. 763-766, 2017.

[27] R. Hao, W. Li, K. Fu, G. Yu, L. Song, J. Yuan, J. Li, X. Deng, X. Zhang, Q. Zhou, Y. Fan, W. Shi, Y. Cai, X. Zhang, B. Zhang, "Breakdown enhancement and current collapse suppression by high-resistivity GaN cap layer in normally-off AlGaN/GaN HEMTs", *IEEE Electron Device Letters*, vol. 38, no.11, pp. 1567-1570, 2017.

[28] B. Duan, S. Xie, H. Guo, Y. Yang, "Etched $Al_{0.32}Ga_{0.68}N$/GaN HEMTs with high output current and breakdown voltage (> 600 V)", *Micro & Nano Letters*, vol. 13, no.5, pp. 676-679, 2018.

[29] T. Kabemura, S. Ueda, Y. Kawada, K. Horio, "Enhancement of Breakdown Voltage in AlGaN/GaN HEMTs: Field Plate Plus High-k Passivation Layer and High Acceptor Density in Buffer Layer", *IEEE Transactions on Electron Devices*, vol. 65, no.9, pp. 3848-3854, 2018.

[30] G. Zhou, Z. Wan, G. Yang, Y. Jiang, R. Sokolovskij, H. Yu, G. Xia, "Gate leakage suppression and breakdown voltage enhancement in p-GaN HEMTs using metal/graphene gates", *IEEE Transactions on Electron Devices*, vol. 67, no.3, pp. 875-880, 2020.

[31] S. Yuan, B. Duan, X. Yuan, Z. Cao, H. Guo, Y. Yang, "New $Al_{0.25}Ga_{0.75}N$/GaN high electron mobility transistor with partial etched AlGaN layer", *Superlattices and Microstructures*, vol. 93, pp. 303-307, 2016.

[32] Y. Liu, Q. Yu, J. Du, "Simulation design of a high-breakdown-voltage p-GaN-gate GaN HEMT with a hybrid AlGaN buffer layer for power electronics applications", *Journal of Computational Electronics*, vol. 19, pp. 1527-1537, 2020.

[33] P. Srivastava, J. Das, D. Visalli, J. Derluyn, M.V. Hove, P.E. Malinowski, D. Marcon, K. Geens, K. Cheng, S. Degroote, M. Leys, M. Germain, S. Decoutere, R.P. Mertens, G. Borghs, "Silicon substrate removal of GaN DHFETs for enhanced (< 1100 V) breakdown voltage", *IEEE Electron Device Letters*, vol. 31, no.8, pp. 851-853, 2010.

[34] J. Liu, Y.-F. Guo, J. Zhang, J. Yao, M. Zhang, C. Huang, L. Du, "Analytical Study on the Breakdown Characteristics of Si-Substrated AlGaN/GaN HEMTs With Field Plates", *IEEE Journal of the Electron Devices Society*, **8**: pp. 1031-1038, 2020.

[35] H. Wu, B.-X. Duan, L.-Y. Yang, Y.-T. Yang, "Theoretical analytic model for RESURF AlGaN/GaN HEMTs", *Chinese Physics B*, vol. 28, no.2, pp. 027302, 2019.

[36] M. Kaddeche, A. Telia, A. Soltani, “Analytical modeling and analysis of $Al_mGa_{1-m}N$/GaN HEMTs employing both field-plate and high-k dielectric stack for high-voltage operation”, *Journal of Computational Electronics*, vol.12, no.3, pp. 501-510, 2013.
[37] M. Wei, S.W.-Bo, Y. Cui, Z. Chao, Z.J.-Cheng, M.X.- Hua, Z.J.- Feng, L.H.- Xia, Y.L.- An, Z. Kai, Z. S.-Lei, C.Y.- He, Z.X.- Feng, H. Yue, “A two-dimensional fully analytical model with polarization effect for off-state channel potential and electric field distributions of GaN-based field-plated high electron mobility transistor”, *Chinese Physics B*, vol.23, no.8, pp. 087305-8, 2014.
[38] T. Chen, Q. Zhou, D. Wei, C. Dong, W. Chen, B. Zhang, “Physics-based 2-D analytical model for field-plate engineering of AlGaN/GaN power HFET”. *IEEE Transactions on Electron Devices*, vol.66, no.1, pp. 116-125, 2018.
[39] J. Liu, Y. Guo, J. Zhang, J. Yao, X. Huang, C. Huang, Z. Huang, K. Yang, “Analytical model for the potential and electric field distributions of AlGaN/GaN HEMTs with gate-connected FP based on equivalent potential method”, *Superlattices and Microstructures*, vol.138, pp. 106327-106342, 2020.

[40] L. Yang, B. Duan, Y. Wang, Y. Yang, “Analytical models for the electric field and potential of AlGaN/GaN HEMT with partial silicon doping”, *Superlattices and Microstructures*, vol.128, pp. 349-357, 2019.

[41] G. Haijun, D. Baoxing, W. Hao, Y. Yintang, “Analytical model of AlGaN/GaN HEMTs with a partial GaN cap layer”, *Superlattices and Microstructures*, vol.123, pp. 210-217, 2018.

[42] S.M. Razavi, S.H. Zahiri, S.E. Hosseini, “A novel AlGaN/GaN HEMT with a p-layer in the barrier”, *Physica E: Low-dimensional Systems and Nanostructures*, vol.54, pp. 24-29, 2013.

[43] S.P. Kumar, A. Agrawal, R. Chaujar, M. Gupta, R.S. Gupta, “Analytical modeling and simulation of subthreshold behavior in nanoscale dual material gate AlGaN/GaN HEMT”, *Superlattices and Microstructures*, vol.44, no.1, pp. 37-53, 2008.

[44] فرهاد عباس نژاد، مجید طیرانی، ادیب ابریشمی فر و احسان جوهری سلماسی "بهبود مشخصه های خطینگی تقویت کننده های توان GaN بر مبنای تزریق سیگنال هارمونیک دوم" مجله مهندسی برق دانشگاه تبریز، جلد ۵۱، شماره ۴، صفحات ۴۱۲-۴۰۴، ۱۴۰۰.

[45] سارا سجادی، محمد سروش، کریم انصاری اصل، " پیشنهاد یک طرح جدید به منظور افزایش بازده دیود گسیل نور گالیم نیتراید مبتنی بر بلور فوتونی" مجله مهندسی برق دانشگاه تبریز، جلد ۴۸، شماره ۳، ۱۳۹۷.
[46] H.X. Guang, Z.D. Gang, J.D. Sheng, “Formation of two-dimensional electron gas at AlGaN/GaN heterostructure and the derivation of its sheet density expression”, *Chin. Phys. B*, vol.24, no.6, pp. 067301-5, 2015.